Graphic Optimization Method of Crowdsourcing Trajectories Using Geomagnetic Field and Map Loop Closures

Zilin Hong[1,2], Wen Li[1,*], Yupeng Xia[1,2], Dongyan Wei[1] and Ge Shen[1]

[1]Aerospace Information Research Institute, Chinese Academy of Sciences, Beijing 100094, China
[2]School of Electronic, Electrical and Communication Engineering, University of Chinese Academy of Science, Beijing 100049, China

Abstract

Mobile crowdsourcing enables large-scale construction and updating of fingerprint databases for indoor positioning (e.g., Wi-Fi, geomagnetic). Accurate trajectory recovery from such data, however, remains challenging due to cumulative dead-reckoning (DR) errors, susceptibility to local optima, and rapid drift in vehicular scenarios. This paper presents a graph optimization framework that refines crowdsourced trajectories by integrating three types of constraints: (1) adjacent-pose constraints from a smartphone GNSS/MEMS DR filter enhanced with an empirical velocity model to mitigate indoor drift; (2) relative loop closures detected via geomagnetic sequence matching, exploiting the spatial stability of indoor geomagnetic fields; and (3) absolute loop closures obtained from OpenStreetMap (OSM) map matching to enforce global consistency. A joint graph optimization using these constraints produces globally refined trajectories. Experiments in two underground parking garages with multiple smartphones show that, compared with single-constraint approaches, the proposed method achieves clear improvements in trajectory accuracy.

Keywords

indoor positioning, mobile crowdsourcing, graph optimization, geomagnetic sequence matching, map matching

1. Introduction

Mobile crowdsourcing is a key technology for dynamic mapping and updating in fingerprint-based indoor positioning systems, enabling large-scale applications such as Wi-Fi and geomagnetic matching. The core challenge is obtaining fine-grained and accurate fingerprint location annotations, which directly determine the positioning accuracy of the fingerprint database [1]. Precise recovery of indoor trajectories from crowdsourced data is central to building indoor fingerprint maps.

Previous research has explored various approaches. Wi-Fi-based crowdsourced mapping [2] is limited in areas with poor Wi-Fi coverage. Pedestrian dead reckoning (PDR) combined with clustering [3] suffers from cumulative drift due to lack of absolute positional information. Geomagnetic-based methods [4] leverage inherent indoor magnetic features for trajectory correction. Integration of geomagnetic fields with extended Kalman filter (EKF)-based dead reckoning [5] improves accuracy but relies on epoch-by-epoch estimation, risking local optima. Recent work combines geomagnetic SLAM loop closure with graph optimization (G2O) [6] or frequency-domain geomagnetic features [7] to enhance global trajectory consistency.

Analysis suggests that exploiting the spatial stability of indoor geomagnetic fields to construct loop closure points, in combination with optimizing crowdsourced DR trajectories, can effectively enhance the accuracy of indoor trajectory recovery. However, two challenges remain:

IPIN-WCAL 2025: Workshop for Computing & Advanced Localization at the Fifteenth International Conference on Indoor Positioning and Indoor Navigation, September 15–18, 2025, Tampere, Finland

*Corresponding author.
h2714450470@163.com (Z. Hong); wen.li@aircas.ac.cn (W. Li); xiayupeng22@mails.ucas.ac.cn (Y. Xia); weidy@aircas.ac.cn (D. Wei); shenge@aircas.ac.cn (G. Shen)
https://people.ucas.ac.cn/~wen.li (W. Li); https://people.ucas.ac.cn/~0041454 (D. Wei); https://people.ucas.edu.cn/~0053135 (G. Shen)

1. DR-based pose constraints and geomagnetic loop closures are relative spatial constraints, risking local optima in graph optimization.
2. Initial DR trajectories are critical. Pedestrian DR can leverage zero-velocity or step-length constraints, but vehicle-based crowdsourced DR rapidly diverges due to high speeds and lack of effective velocity constraints, undermining pose reliability between consecutive timestamps.

To address these challenges, this paper proposes a crowdsourced trajectory graph optimization framework integrating three constraints. First, a smartphone GNSS/MEMS integrated navigation and DR filter with an empirical velocity model extrapolates outdoor trajectories indoors, producing coarse indoor trajectories and adjacent-pose constraints. Second, an improved dynamic time warping (DTW) algorithm detects geomagnetic loop closures within and between trajectories, establishing relative loop constraints. Third, outdoor map constraints are extracted from OpenStreetMap (OSM) via an HMM-based map-matching algorithm, providing absolute loop closures to enhance global consistency during G2O optimization.

Finally, the joint graph optimization is solved using the Levenberg–Marquardt (LM) algorithm. By incorporating absolute loop closure constraints alongside relative constraints and introducing an empirical vehicle speed model in the DR filter, the method prevents convergence to local optima and mitigates rapid divergence in indoor DR, improving the reliability of pose constraints between consecutive timestamps.

2. Algorithm Framework

The proposed method constructs a G2O-based graph optimization model with three types of constraints to refine indoor crowdsourced trajectories. The overall workflow, illustrated in Figure 1, comprises the following steps:

1. **Adjacent Pose Constraints:** A smartphone's GNSS and MEMS sensors (accelerometer, gyroscope) are integrated in a navigation and DR filter to extrapolate trajectories from outdoor to indoor environments, producing coarse indoor trajectories. Adjacent pose constraints are derived from these trajectories.
2. **Geomagnetic Loop Closure Constraints:** Geomagnetic measurements are corrected for hard/-soft iron interference using quasi-static azimuth compensation. An improved dynamic time warping (DTW) algorithm detects loop closures within and across trajectories, forming geomagnetic loop closure constraints.
3. **Map-Matching Constraints:** Key points of indoor DR trajectories (e.g., entrances/exits) are aligned with outdoor trajectories and OSM road lines via map matching, providing absolute positional constraints.
4. **Backend Graph Optimization:** All constraints are integrated into a unified graph. The Levenberg-Marquardt (LM) algorithm iteratively solves for the globally optimal trajectory, yielding refined indoor coordinates.

This framework leverages smartphone sensor data and open-source maps, ensuring wide applicability.

3. Algorithm Description

3.1. Adjacent Pose Constraints

This study extends the smartphone GNSS/MEMS/OBD integrated filtering method [8] by proposing a hybrid odometry model that replaces OBD-derived speed constraints in non-cooperative crowdsourcing. A segmented velocity framework uses GNSS outdoors and empirical velocity indoors, enabling seamless trajectory extrapolation without OBD hardware.

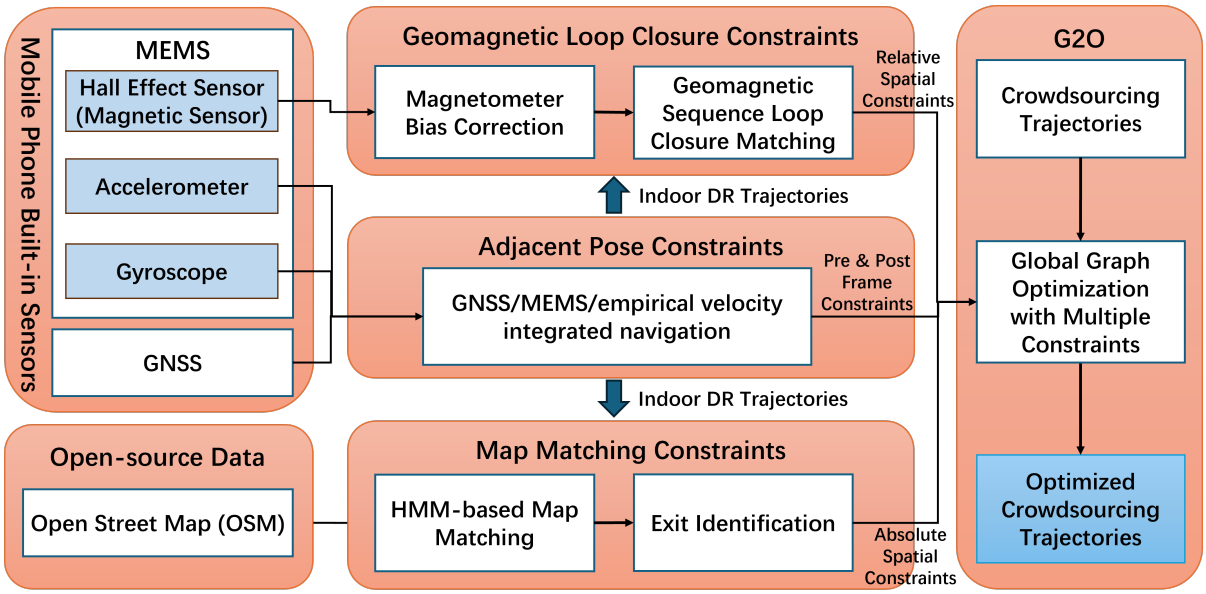

Figure 1: Framework of crowdsourced trajectory optimization algorithms.

The filter state vector includes attitude, velocity, position errors, and sensor biases:

$$\boldsymbol{X} = \left[\delta\boldsymbol{\phi}, \delta\boldsymbol{v}, \delta\boldsymbol{P}, \boldsymbol{\nabla}_a, \boldsymbol{\varepsilon}_g\right]^{\mathrm{T}}, \tag{1}$$

where $\delta\boldsymbol{\phi}$, $\delta\boldsymbol{v}$, and $\delta\boldsymbol{P}$ are attitude, velocity, and position errors, respectively, and $\boldsymbol{\nabla}_a$, $\boldsymbol{\varepsilon}_g$ denote accelerometer and gyroscope biases.

Observation equations incorporate multiple sources: GNSS when available, otherwise MEMS-based motion constraints. Indoors, empirical velocity v_{est} guides state updates through motion constraints. The state vector is sequentially updated via Kalman filtering.

Adjacent position and attitude constraints are derived from the indoor dead reckoning trajectory to ensure local continuity and overall trajectory consistency in subsequent optimization.

3.2. Geomagnetic Loop Closure Constraints

3.2.1. Magnetometer Bias Correction

In vehicle-mounted scenarios, smartphone magnetometers are affected by non-orthogonal errors, scale factor errors, zero-bias errors, and vehicle-induced magnetic interference. Calibration is thus essential prior to geomagnetic loop closure detection. A simplified linear model is adopted, and ellipsoid fitting tests indicate that zero-bias errors dominate. The model is expressed as

$$\boldsymbol{B}_{\mathrm{e}} = \boldsymbol{B}_{\mathrm{m}} - \boldsymbol{d}, \tag{2}$$

where $\boldsymbol{B}_{\mathrm{m}}$ is the raw measurement, $\boldsymbol{d}$ is the zero-bias vector, and $\boldsymbol{B}_{\mathrm{e}}$ is the calibrated measurement.

Using the vehicle heading from GNSS and the horizontal geomagnetic components, the zero-bias parameters are estimated under a quasi-static geomagnetic field and known local declination [9]. Three-axis measurements are projected onto the body frame, and the bias is solved via least-squares, ensuring consistency across smartphones and improving geomagnetic loop closure accuracy.

3.2.2. Geomagnetic Sequence Loop Closure Matching

To solve the problem of non-uniform geomagnetic field sequence matching caused by changes in vehicle speed, this paper uses an improved head-tail unconstrained DTW algorithm [6] to perform loop

matching of geomagnetic sequences within and between trajectories:

$$\begin{cases} \mathbf{T}^{(p,q)} = (\mathbf{T}_p, \ldots, \mathbf{T}_q), \\ D_{OBE}(\mathbf{T}_w, \mathbf{T}) = \min D(\mathbf{T}_w, \mathbf{T}^{(p,q)}) \quad \text{subject to } 1 \le p \le q \le M \end{cases}, \tag{3}$$

where $\mathbf{T}_w$ denotes the sliding window of the geomagnetic sequence to be matched from the current trajectory, and $\mathbf{T}$ represents the reference geomagnetic sequence from historical or other trajectories. $\mathbf{T}^{(p,q)}$ refers to an arbitrary subsequence of $\mathbf{T}$, spanning from the p-th to the q-th geomagnetic vector, and D_{OBE} is the optimal head-tail unconstrained DTW distance.

The head-tail unconstrained DTW algorithm compensates for nonlinear temporal variations and speed-induced scale deviations, enabling flexible subsegment matching.

For crowdsourced trajectories, geomagnetic sequence loop closure matching uses this method, with final points obtained via distance-weighted averaging.

3.3. Map Matching Constraints

The first two types of constraints provide only relative positional information, which can reduce relative trajectory error but may still allow overall drift. To improve absolute spatial accuracy, OpenStreetMap (OSM) is introduced to supply absolute positional references. Map-matched points from outdoor trajectory segments form a third type of constraint, jointly optimized with relative constraints to ensure global consistency.

OSM road segments are represented as straight-line polylines, while real vehicle trajectories may include curved turns. Straight segments are identified via curve detection, and an improved HMM-based map-matching algorithm [10] aligns trajectory points with OSM features. Transition points where GNSS signals reappear (e.g., indoor-to-outdoor) are also used as positional constraints.

The vehicle trajectory is denoted as $\boldsymbol{X} = \{\boldsymbol{x}_1, \ldots, \boldsymbol{x}_t\}$, with each $\boldsymbol{x}_i$ containing 2D coordinates and heading. Reference points $\boldsymbol{S} = \{\boldsymbol{s}_1, \ldots, \boldsymbol{s}_n\}$ are interpolated from OSM segments, each with geographic coordinates and a road segment ID.

The observation probability between a trajectory point $\boldsymbol{x}_i$ and reference point $\boldsymbol{s}_j$ is modeled as

$$P(\boldsymbol{o}_t \mid \boldsymbol{s}_j) = \exp\Big(-\frac{d_{ij}^2}{2\sigma^2}\Big), \tag{4}$$

where $\boldsymbol{o}_t$ is the observation at time t, d_{ij} is the Euclidean distance, and σ reflects expected positioning error.

The state transition probability between consecutive reference points $\boldsymbol{s}_j$ and $\boldsymbol{s}_k$ is

$$P(\boldsymbol{s}_j \mid \boldsymbol{s}_k) = \begin{cases} \exp\left(-\frac{d_{jk}^2}{2\sigma^2}\right), & \text{if on the same road} \\ \exp\left(-\frac{d_{jk}}{\sigma}\right), & \text{otherwise} \end{cases}, \tag{5}$$

assigning higher probability to transitions along the same road.

Finally, the Viterbi algorithm computes the most likely sequence of matched points:

$$dp[j,t] = \max_k \big(dp[k, t-1] \cdot P(\boldsymbol{s}_j \mid \boldsymbol{s}_k)\big) \cdot P(\boldsymbol{o}_t \mid \boldsymbol{s}_j), \tag{6}$$

where $dp[j,t]$ denotes the maximum likelihood at reference point $\boldsymbol{s}_j$ at time t. The resulting matched points are then used as constraints in the graph-based optimization framework.

3.4. Backend Graph Optimization

The backend graph optimization refines trajectory estimates by jointly incorporating multiple constraints. A trajectory p with l poses at the k-th iteration is denoted as

$$\boldsymbol{X}_p^k = \left\{\boldsymbol{x}_{p_1}^k, \boldsymbol{x}_{p_2}^k, \ldots, \boldsymbol{x}_{p_l}^k\right\}, \tag{7}$$

where each pose $\boldsymbol{x}_{p_i}^k = \left[x_{p_i}^k, y_{p_i}^k, \theta_{p_i}^k\right]^\top$ consists of 2D coordinates and a heading angle.

The global nonlinear least-squares objective over all trajectories is formulated as

$$F(\boldsymbol{X}) = \sum_{(i,j)\in\boldsymbol{C}} \boldsymbol{e}_{i,j}^\top \boldsymbol{\Omega}_{ij} \boldsymbol{e}_{i,j}, \tag{8}$$

where $\boldsymbol{X}$ denotes the set of all poses, $\boldsymbol{e}_{i,j}$ the residual between vertices i and j, $\boldsymbol{\Omega}_{ij}$ the information matrix weighting constraint confidence, and $\boldsymbol{C}$ the set of adjacent-pose, geomagnetic loop-closure, and map-matching constraints.

The adjacent-pose constraint enforces smooth motion between consecutive poses, with residual

$$\boldsymbol{e}_{i,i+1}^{\text{adj}} = \begin{bmatrix} \Delta x_{p_i,p_{i+1}}^0 - \Delta \hat{x}_{p_i,p_{i+1}}^k \\ \Delta y_{p_i,p_{i+1}}^0 - \Delta \hat{y}_{p_i,p_{i+1}}^k \\ \Delta \theta_{p_i,p_{i+1}}^0 - \Delta \hat{\theta}_{p_i,p_{i+1}}^k \end{bmatrix}, \tag{9}$$

where the superscript 0 denotes observations and $\hat{\cdot}$ denotes estimates at iteration k.

Geomagnetic loop-closure constraints include intra-trajectory loops,

$$\boldsymbol{e}_{i,j}^{\text{loop}} = \begin{bmatrix} -\Delta \hat{x}_{i,j}^p \\ -\Delta \hat{y}_{i,j}^p \\ -\Delta \hat{\theta}_{i,j}^p \end{bmatrix}, \tag{10}$$

and inter-trajectory loops between trajectories p and q,

$$\boldsymbol{e}_i^{\text{mag}} = \begin{bmatrix} -\Delta \hat{x}_{p_i,p_j}^k \\ -\Delta \hat{y}_{p_i,p_j}^k \end{bmatrix}. \tag{11}$$

For map-matching, residuals are defined with respect to OSM reference points as

$$\boldsymbol{e}_i^{\text{osm}} = \begin{bmatrix} -\Delta \hat{x}_{p_i,\text{osm}_j}^k \\ -\Delta \hat{y}_{p_i,\text{osm}_j}^k \end{bmatrix}. \tag{12}$$

The complete objective function for $n \geq 2$ trajectories is

$$F(\boldsymbol{X}_n) = \sum \boldsymbol{e}_{i,j}^{\text{adj}} \boldsymbol{\Omega}_{ij} \boldsymbol{e}_{i,j}^{\text{adj}} + \sum \boldsymbol{e}_{i,j}^{\text{loop}} \boldsymbol{\Omega}_{ij}^{\text{loop}} \boldsymbol{e}_{i,j}^{\text{loop}} + \sum \boldsymbol{e}_i^{\text{mag}} \boldsymbol{\Omega}_{ij}^{\text{mag}} \boldsymbol{e}_i^{\text{mag}} + \sum \boldsymbol{e}_i^{\text{osm}} \boldsymbol{\Omega}_{ij}^{\text{osm}} \boldsymbol{e}_i^{\text{osm}}. \tag{13}$$

For single-trajectory cases ($n = 1$), the inter-trajectory geomagnetic term is omitted.

The optimal trajectory is obtained by minimizing $F(\boldsymbol{X}_n)$ with the Levenberg–Marquardt algorithm [11]:

$$\boldsymbol{X}_n^* = \arg\min_{\boldsymbol{X}_n} F(\boldsymbol{X}_n). \tag{14}$$

This optimization yields globally consistent trajectories by jointly balancing all constraint types.

4. Experiments and Evaluation

4.1. Experimental Setup

The experiments were conducted in two underground parking structures and adjacent urban-canyon roadways in Haidian District, Beijing. Figure 2(a) shows the street view at the entrance of Scenario 1, flanked by high-rise buildings that create a typical urban-canyon environment with severe multipath and non-line-of-sight (NLOS) GNSS effects. Figure 2(b) presents a remote-sensing image of Scenario 2, highlighting the underground parking structure and its surrounding roadways where the experiments were carried out.

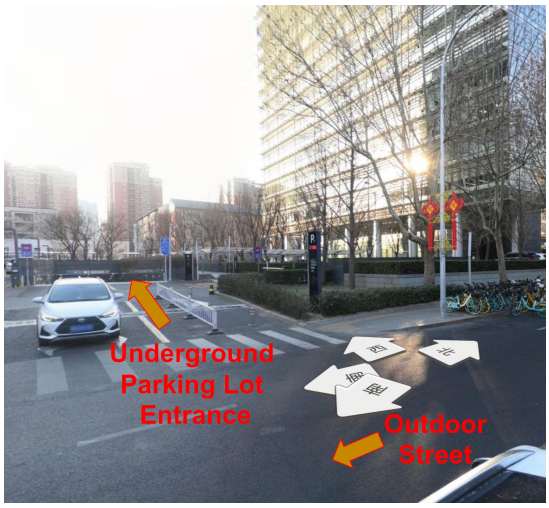

(a) Scenario 1: urban canyon at parking entrance
Source: Baidu Map (https://map.baidu.com/)

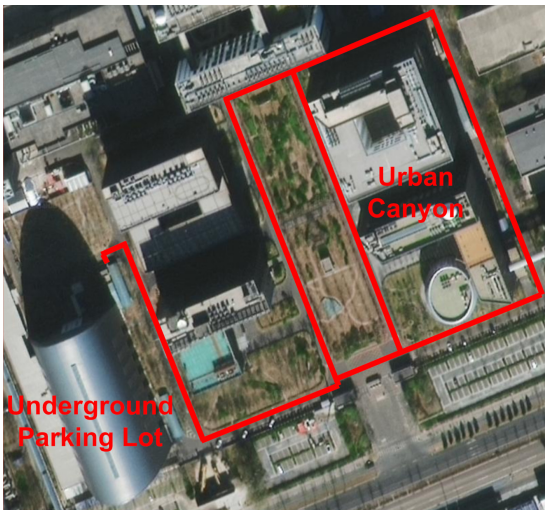

(b) Scenario 2: underground parking and roadways
Source: Baidu Map (https://map.baidu.com/)

(c) Data acquisition interface and mounting setup

(d) Crowdsourced smartphone models

Figure 2: Experimental scenarios and equipment. (a) Scenario 1; (b) Scenario 2; (c) Data interface and mounting; (d) Crowdsourced smartphones.

Test data were collected using two smartphones vivo X100 and iQOO Z9, both supporting dual-frequency L1/L5 GNSS and tri-axial MEMS IMUs. Figure 2(c) shows the multi-sensor data acquisition software interface and the mounting configuration of the devices. Each device was rigidly mounted in a strapdown setup on the front interior of the vehicle, below the windshield, with the Y-axis aligned to the forward direction, the X-axis to the vehicle right-hand side, and the Z-axis upward, thereby fixing the relation between the phone body frame and the vehicle frame.

Before each test, the vehicles remained stationary for 30 s to collect static IMU data, enabling offline estimation of gyroscope and accelerometer biases as well as magnetometer calibration.

In addition to these test devices, the crowdsourced database was constructed from nine different smartphones, including Huawei Mate60Pro, Huawei Mate20, Xiaomi14, and Honor Magic6, providing diverse sensor data for trajectory optimization (Figure 2(d)).

4.2. Experimental Results

Figure 3 illustrates integrated navigation trajectories from crowdsourced smartphone data under different optimization strategies. Scenario 1 (left column) and Scenario 2 (right column) correspond to two representative locations within urban canyon and underground parking environments.

In each scenario, the gray lines represent the GNSS/MEMS baseline trajectory. The first row of subfigures (a, b) shows OSM map matching results, the second row (c, d) presents geomagnetic sequence matching results, and the third row (e, f) depicts the joint G2O optimization combining both constraints (G2O(Mag & Map)). In the visualizations, red lines correspond to G2O with geomagnetic-only constraints (G2O(Mag)), green lines denote G2O with map-only constraints (G2O(Map)), and blue lines indicate the proposed joint optimization. Black lines show the OpenStreetMap (OSM) reference.

The results demonstrate that G2O(Mag & Map) yields the most consistent trajectories across indoor and outdoor areas. In the indoor parking lot (yellow box), where GNSS is severely degraded, G2O(Map) reduces drift but exhibits misalignments, whereas G2O(Mag) improves indoor loop closures but underperforms outdoors due to weak geomagnetic features. By integrating both constraints, G2O(Mag & Map) minimizes indoor errors relative to G2O(Map) and outdoor errors relative to G2O(Mag), producing trajectories closely aligned with the OSM map.

These results confirm that the joint optimization effectively balances the strengths of individual constraints, resulting in more accurate and reliable navigation in complex urban environments.

5. Conclusion

This paper addresses the challenge of precise indoor trajectory recovery from mobile crowdsourced data by proposing a graph optimization framework leveraging geomagnetic and map-based loop closure constraints. The methodology proceeds as follows:

1. A smartphone GNSS/MEMS integrated navigation and dead-reckoning (DR) filter, enhanced with an empirical velocity model, extrapolates trajectories from outdoor to indoor environments. This generates coarse indoor trajectories and establishes adjacent-pose constraints.
2. Exploiting the spatial stability of indoor geomagnetic fields, an improved dynamic time warping (DTW) algorithm detects loop closures within and across trajectories, forming relative loop-closure constraints.
3. Outdoor map constraints are obtained from OpenStreetMap (OSM) via a hidden Markov model (HMM)-based map-matching algorithm. These absolute loop closures enhance global consistency during G2O optimization.
4. A joint graph optimization model integrates adjacent-pose, geomagnetic loop, and map-matching constraints, which is solved using the Levenberg-Marquardt (LM) algorithm to yield globally optimized trajectories.

The main contributions are:

1. While existing geomagnetic loop closure-based methods rely solely on relative spatial constraints and risk convergence to local optima, the proposed approach incorporates absolute spatial references—such as entrance/exit points and OSM map-matching points—into the G2O loss function, improving optimization robustness.
2. To mitigate rapid divergence of indoor DR trajectories due to lack of external velocity references, the empirical velocity model in the GNSS/MEMS filter provides reliable extrapolation from outdoor to indoor trajectories. This generates adjacent-pose constraints that preserve consistent pose relationships between consecutive trajectory points, ensuring continuous indoor trajectory recovery for crowdsourced data.

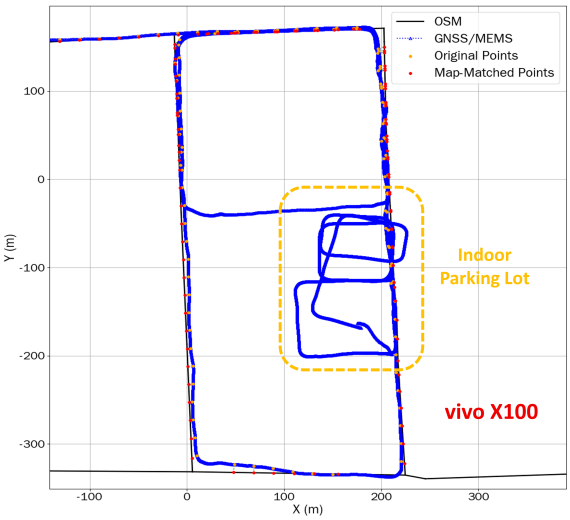

(a) Scenario 1: Map matching

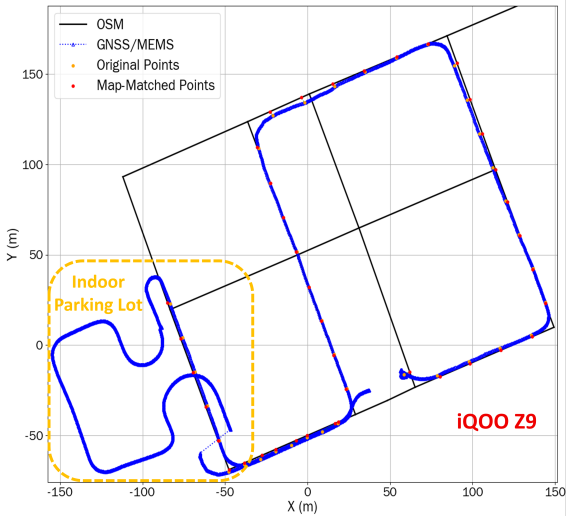

(b) Scenario 2: Map matching

(c) Scenario 1: Geomagnetic loop closure

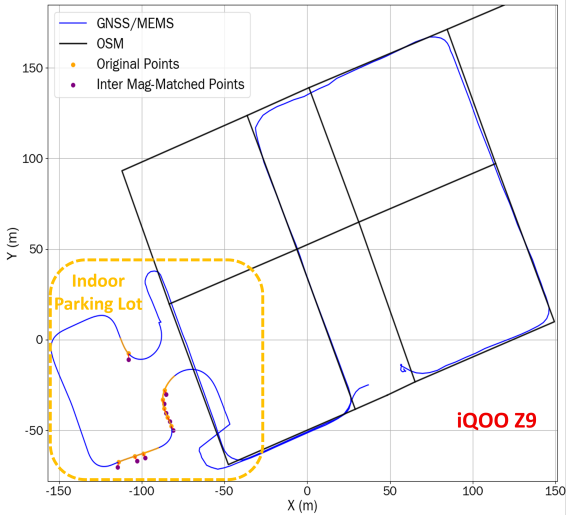

(d) Scenario 2: Geomagnetic loop closure

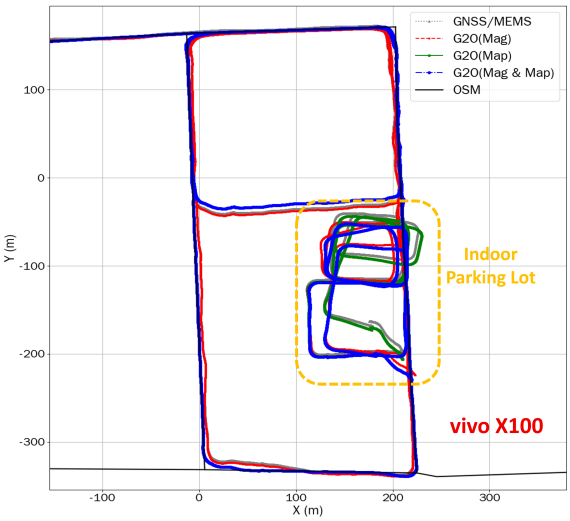

(e) Scenario 1: Joint graph optimization

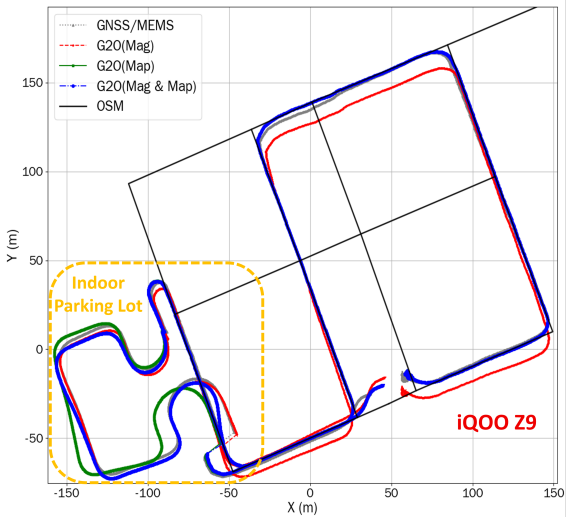

(f) Scenario 2: Joint graph optimization

Figure 3: Crowdsourced trajectory optimization results based on G2O. (a)(b) OSM map matching; (c)(d) Geomagnetic sequence matching; (e)(f) G2O joint optimization.

Declaration on Generative AI

During the preparation of this work, the author(s) used the following generative AI tools:

- **ChatGPT-5 (OpenAI)**: Used for grammar and spelling checks.
- **Kimi-1.5 (Moonshot AI)**: For generating LaTeX versions of equations.

After using these tools, the author(s) reviewed, verified, and edited the content as needed, and take(s) full responsibility for the publication's content.

References

[1] B. Lashkari, J. Rezazadeh, R. Farahbakhsh, K. Sandrasegaran, Crowdsourcing and sensing for indoor localization in iot: A review, IEEE Sensors Journal 19 (2018) 2408–2434.

[2] W. Li, D. Wei, Q. Lai, X. Li, H. Yuan, Geomagnetism-aided indoor wi-fi radio-map construction via smartphone crowdsourcing, Sensors 18 (2018) 1462.

[3] A. Ayanoglu, D. M. Schneider, B. Eitel, Crowdsourcing-based magnetic map generation for indoor localization, in: 2018 International Conference on Indoor Positioning and Indoor Navigation (IPIN), IEEE, 2018, pp. 1–8.

[4] L. Chen, J. Wu, C. Yang, Meshmap: A magnetic field-based indoor navigation system with crowdsourcing support, IEEE Access 8 (2020) 39959–39970.

[5] Y. Li, Z. He, Z. Gao, Y. Zhuang, C. Shi, N. El-Sheimy, Toward robust crowdsourcing-based localization: A fingerprinting accuracy indicator enhanced wireless/magnetic/inertial integration approach, IEEE Internet of Things Journal 6 (2018) 3585–3600.

[6] B. Yao, W. Li, D. Wei, X. Ji, W. Zhang, Robust magnetic field loop closure detection for low-cost robot's localization and mapping, in: China Satellite Navigation Conference (CSNC 2022) Proceedings: Volume III, Springer, 2022, pp. 541–551.

[7] Y. Wang, J. Kuang, T. Liu, X. Niu, J. Liu, Crowdmagmap: Crowdsourcing-based magnetic map construction for shopping mall, IEEE Internet of Things Journal 11 (2023) 5362–5373.

[8] J. Xinchun, W. Dongyan, Y. Hong, Z. Deyun, Vehicle multi-source fusion navigation method based on smartphone platform, J. Chin. Inertial Technol. 28 (2020) 638–644.

[9] L. Yuxin, L. Wen, W. Dongyan, J. Xinchun, S. Ge, Online calibration method of smartphone magnetometer in vehicle geomagnetic matching positioning, in: 2022 IEEE 12th International Conference on Indoor Positioning and Indoor Navigation (IPIN), IEEE, 2022, pp. 1–8.

[10] P. Newson, J. Krumm, Hidden markov map matching through noise and sparseness, in: Proceedings of the 17th ACM SIGSPATIAL international conference on advances in geographic information systems, 2009, pp. 336–343.

[11] R. Kümmerle, G. Grisetti, H. Strasdat, K. Konolige, W. Burgard, g 2 o: A general framework for graph optimization, in: 2011 IEEE international conference on robotics and automation, IEEE, 2011, pp. 3607–3613.